Phase transitions in de Sitter spacetimes: Quantum Corrections

José Eliel Camargo-Molina,[1] Mariana Carrillo González,[2] and Arttu Rajantie[2]
[1]Department of Physics and Astronomy, Uppsala University, Box 516, SE-751 20 Uppsala, Sweden
[2]Theoretical Physics, Blackett Laboratory, Imperial College, London SW7 2AZ, United Kingdom

(Received 28 April 2022; accepted 16 February 2023; published 20 March 2023)

We investigate the decay rate of a false vacuum state in de Sitter space at high Hubble rates, using two methods: the Hawking-Moss instanton method which is fully quantum mechanical but relies on the saddle-point approximation, and the Starobinsky-Yokoyama stochastic approach which is nonperturbative but does not include quantum effects. We use the flux over population method to compute the Hawking-Moss decay rate at one-loop order, and demonstrate that in its domain of validity, it is reproduced by the stochastic calculation using the one-loop constraint effective potential. This suggests that the stochastic approach together with the constraint effective potential can be used to accurately describe vacuum decay beyond the saddle-point approximation.

DOI: 10.1103/PhysRevD.107.063533

I. INTRODUCTION

A ubiquitous phenomenon of quantum field theories is quantum tunneling which renders a classically stable vacuum metastable and leads to phase transitions. Precision calculations of the decay rate of such metastable vacuum are relevant for understanding and constraining possible physics beyond the standard model (SM) and nonminimal gravitational couplings. Given the current measurements of the SM Higgs and top quark masses [1,2], our Universe seems to lie in a metastable state which should have a small enough decay rate [3–7]. In the early Universe the decay rate can be enhanced by different mechanisms [8]; hence, rigorous calculations of such decay rates are important to understand the constraints on new physics.

In flat space, a formal definition of the decay rate of the false vacuum is given by $\Gamma = -2\mathrm{Im}(E) = 2\mathrm{Im}(\lim_{T\to\infty}(\ln Z)/T)$, where Z is the path integral. The decay rate per unit volume can be computed using the saddle-point approximation which at next-to-leading (NLO) gives [9,10]

$$\frac{\Gamma}{\mathcal{V}} = \left(\frac{B}{2\pi}\right)^2 \left|\frac{\det' S''(\phi_b)}{\det S''(\phi_{\mathrm{fv}})}\right|^{-1/2} e^{-B} \tag{1.1}$$

where ϕ_b is the saddle-point or *bounce*, ϕ_{fv} is the false vacuum, the prime on the determinant indicates that only nonzero modes are included, $B = S(\phi_b) - S(\phi_{\mathrm{fv}})$, and S is the Euclidean action. Note that the functional determinant ratio is divergent and can be regularized using standard QFT methods. Classically, the false vacuum is well defined as a local minimum of the potential given by $\phi(x) = \phi_{\mathrm{fv}}$. Quantum mechanically, we require that the false vacuum satisfies $\langle\phi(x)\rangle = \phi_{\mathrm{fv}}$, in addition to its wave function being localized at ϕ_{fv}. Since tunneling is allowed, a wave function localized in the false vacuum does not correspond to an eigenstate of the Hamiltonian. Thus, the false vacuum is a metastable state with complex energy whose imaginary part is proportional to the decay rate [11,12].

A formal definition of the decay rate in curved spacetimes is not available, yet one can push forward by making analogies with the flat space result. At high curvatures, this analogy breaks down, but it has been argued [13] that one can use a thermal interpretation of de Sitter (dS) spacetime instead to define the decay rate. In this letter, we compute one-loop quantum corrections using the thermal interpretation and show that the stochastic Starobinsky-Yokoyama effective theory can then be used to compute the decay rate including these corrections. We argue that this result is valid even beyond the saddle-point approximation.

II. DECAY RATE IN DS SPACE

In the following, we will focus on decays in fixed Sitter backgrounds. The generalization of the decay rate computation to curved spacetimes was proposed in [14]. At small ratios of spacetime curvature to the curvature at the top of the potential barrier ($H/\sqrt{|V''_{\mathrm{top}}|}$) the Coleman-de Luccia bounce is expected to drive the decay [15], but as the spacetime curvature is increased, or the top of the potential barrier becomes more flat, a solution that has no flat space analog takes over, this is the Hawking-Moss instanton [16]. In the large curvature case, the decay rate can also be computed through a different method dubbed the stochastic formalism [17–19]. In the following we give a short review of both approaches. We will focus on computing the one-loop corrections through saddle-point approximation and comparing this result with the stochastic formalism one.

A. Stochastic approach

The stochastic formalism relies on splitting a light quantum field living in a dS space into long (classical) and short (quantum) modes, and describing the latter as stochastic noise. This framework has been shown to be useful for perturbative and nonperturbative quantum field theory computations in dS backgrounds, particularly in addressing issues for light fields [20–23]. Assuming that the long-wavelength modes, ϕ, satisfy an overdamped Langevin equation, it is found that the one-point probability distribution $P(t;\phi)$ of ϕ at time t follows the Fokker-Planck (FP) equation

$$\frac{\partial\tilde{P}(t;\phi)}{\partial t} = \frac{3H^3}{4\pi^2}\tilde{D}_\phi\tilde{P}(t;\phi), \tag{2.1}$$

$$\tilde{D}_\phi = \frac{1}{2}\frac{\partial^2}{\partial\phi^2} - \frac{1}{2}(v'(\phi)^2 - v''(\phi)), \tag{2.2}$$

$$v(\phi) = \frac{4\pi^2}{3H^4}V(\phi), \tag{2.3}$$

$$\tilde{P}(t;\phi) = e^{\frac{4\pi^2 V(\phi)}{3H^4}}P(t;\phi). \tag{2.4}$$

By expanding the probability in terms of the eigenfunctions of the FP equation, it can be found that the decay rate of the false vacuum is given by the lowest nonzero eigenvalue [19,24].

Within the regime of validity of the saddle-point approximation, the decay rate as computed in the stochastic formalism from the lowest nonzero eigenvalue can be equivalently[1] computed through the flux over population method [24] which is described below. Thus, in the saddle-point approximation the decay rate is given by

$$\Gamma^{\text{S.F.}} = \frac{1}{2\pi}\frac{\sqrt{V''_{\text{fv}}|V''_{\text{top}}|}}{3H}e^{-\frac{8\pi^2\Delta V}{3H^4}}. \tag{2.5}$$

Note that this description is intrinsically classical. As we will show in this article, the thermally assisted tunneling approach suggests that one can use the constraint one-loop effective action in the stochastic approach to capture quantum corrections.

B. Thermally-assisted tunneling

1. Bounce solutions in de Sitter

When we include gravity and consider decays from de Sitter to de Sitter, the topology of the bounce solution is assumed to be a 4-sphere with the metric given by $ds^2 = d\xi^2 + \rho(\xi)^2 d\Omega_3^2$, where ρ has zeros at $\xi = 0$ and $\xi = \xi_{\text{max}}$. The bounce satisfies the boundary conditions $\phi'(0) = \phi'(\xi_{\text{max}}) = 0$, and while the field can approach the false vacuum, it actually never reaches it. For simplicity, we will consider a fixed de Sitter background, $\rho = \sin(\xi H)/H$, which corresponds to the analytic continuation of the de Sitter static path. This approximation is justified for small barriers where $\Delta V \equiv V(\phi_{\text{top}}) - V(\phi_{\text{fv}}) \ll V(\phi_{\text{fv}})$. Here, we focus on the Hawking-Moss (HM) solution given by $\phi = \phi_{\text{top}}$. In analogy with flat space, the decay rate is given as

$$\frac{\Gamma}{\mathcal{V}} \sim e^{-B}, \qquad B = \frac{8\pi^2\Delta V}{3H^4}. \tag{2.6}$$

The HM solution describes the transition of a Hubble volume from the false vacuum to the top of the barrier. In a similar manner to the flat space case, this bounce solution describes a decay only when there is a single negative eigenvalue of S''_{HM} which happens as long as[2]

$$H > \sqrt{|V''_{\text{top}}|}/2. \tag{2.7}$$

Thus the HM solution is expected to describe the decay rate at large curvatures, when the Coleman-de Luccia bounce doesn't exist or its properties are different from standard low curvature expectations.

2. Thermal interpretation

When considering tunneling in a fixed de Sitter background, one can interpret the bounce solutions as thermally assisted tunneling. This is possible since in de Sitter spacetimes we can define a temperature [28]

$$T = \frac{H}{2\pi}, \tag{2.8}$$

due to the finiteness of its horizon. To compute the decay rate in dS, we will work within the thermal interpretation proposed by Brown and Weinberg [13] (based on previous results by [29–31]). We start by considering the scalar field living in a fixed dS spacetime whose action can be thought as the thermal effective action where the thermal modes, in this case the gravitons and subhorizon modes, have been integrated out. This effective field theory (EFT) description is appropriate to compute the tunneling rate since the bubble scale, H, is much smaller than the scale of the thermal modes, $M_{\text{Pl}}, 1/\lambda^{\text{subH}}$. Intuitively, the tunneling process can be thought of as consisting of two parts: the first one corresponding to the thermal excitation of states

[1]This equivalence holds when there is only one direction in field space for the false vacuum to decay and as long as we are within in the weak-noise limit [25,26]. An example where the equivalence is not straightforward is treated in Sec. III.

[2]The eigenvalues of S''_{HM} are given by $\lambda_n = n(n+3)H^2 + V''_{\text{top}}$ [27].

localized in the false vacuum with $E > E_{\rm fv}$ and the second one the quantum tunneling.

Formally, the decay rate can be defined as a thermal average given by [29]

$$\Gamma = \frac{1}{Z_{\rm fv}} \int_0^\infty dE e^{-\beta E} \rho(E) \Gamma(E), \tag{2.9}$$

where $\beta = 1/T = (2\pi)/H$, $\rho(E)$ is the density of states, and $\Gamma(E)$ is the tunneling rate for a given energy E. At high temperatures (equivalently, high curvatures), the integral is dominated by the $E > V_{\rm top}$ region, and the decay rate can estimated as [13]

$$\frac{\Gamma^{\rm high\ T}}{\mathcal{V}} \sim \int_{E_{\rm top}}^\infty dE e^{-\beta E} e^{\beta E_{\rm fv}} \sim e^{-\beta(E_{\rm top} - E_{\rm fv})}, \tag{2.10}$$

which agrees with the HM estimate computed from path integral methods in Eq. (2.6) when we identify the potential energy increment in a horizon volume as

$$\Delta E = E_{\rm top} - E_{\rm fv} = \frac{4\pi}{3H_{\rm fv}^3} \Delta V. \tag{2.11}$$

From this, we see that the Hawking-Moss solution can be interpreted as a purely thermal transition where the thermal fluctuations push the field all the way to the top of the potential barrier and then rolls down to the true vacuum [11]. Thus we note that as we increase the temperature, we observe a transition from the Coleman-de Luccia to Hawking Moss driven decay rate.

The result for the decay rate in Eq. (2.6) is missing the prefactor which requires a more careful calculation. Nevertheless, we cannot use a straightforward generalization of Eq. (1.1) since the Hawking-Moss case does not have a clear analogy with flat space decays in the sense that there are no zero modes and the dilute gas approximation cannot be used. Instead, we will perform a more precise calculation by pushing forward the thermal interpretation of the de Sitter static patch [11,13,28,32–34]. For clarity, we want to note that we are only applying the thermal interpretation to the calculation of decay rates mediated by constant field configurations, and not to quantum field theory in de Sitter space in general. This assumption is well motivated since at high temperatures the physics is driven by long-wavelength ($\lambda > H^{-1}$) modes which suggests that we can use a semiclassical approach in this regime [21,32,35–41]. To perform this semiclassical approximation we use the flux over population method for computing escape rates [42–45] which we review below.

3. Semiclassical approximation via flux over population method

We will describe the Hawking-Moss driven decay as a thermal transition as considered in [11,13]. For our purposes, we can consider an effective field theory describing the physics of long wavelength modes which can be described classically. Through a matching procedure one can encode the quantum corrections of the full theory in the EFT operators. Thus, we can compute one-loop corrections by using this semiclassical approximation. We assume that the EFT degrees of freedom are encoded in a scalar field ϕ. This situation has been previously analyzed in [42–46]. In the following, we give a short review with emphasis on our proposal of its application to computing decay rates in de Sitter space. The classicalization of the long wavelength modes leads to a statistical description of the system where the dynamics of the scalar field are governed by the Langevin equation

$$(\partial_t^2 - \nabla^2)\phi(\vec{x},t) + \frac{\partial V(\phi)}{\partial \phi} + \eta \dot{\phi}(\vec{x},t) = \xi(\vec{x},t), \tag{2.12}$$

where the damping coefficient is $\eta = 3H$ and ξ is the Gaussian white noise. The noise encodes the thermal modes that have been integrated out.

Within the classical EFT point of view, the HM decay rate is computed as the escape rate. This is done by using the flux over population method which consists of solving for the dynamics of the scalar field assuming an initial probability distribution localized in the false vacuum which evolves to the equilibrium state. The solution relies on the special boundary conditions given by the steady-state solution which assumes a source behind the false vacuum and a sink right after the top of the barrier so that there is a constant probability current across the barrier. This also guarantees that we only compute the decay of the false vacuum and we do not include contributions from the flux crossing the barrier back to the false vacuum. These extra contributions exist when there is a minimum on the other side of the barrier—that is, the true vacuum—but they do not appear if the potential is unbounded from below on the other side of the barrier. Note also that the temperature cannot grow indefinitely since we require that it is smaller than ΔE to have a well-defined initial state localized at the false vacuum.

By looking at the Euclidean action in the space of field configurations, one can define transition surfaces by the separatrices between gradient flows which splits the regions of field space into metastable, stable, and unstable regions. Here, we will only focus on one of such transition surfaces. The Hawking-Moss solution lies on this surface and corresponds to the mode with the smallest Euclidean action on this surface. Since the flux of probability has a Boltzmann suppression, the largest contribution to the escape rate comes from the HM solution and we can perform a saddle-point approximation of the Euclidean action. The escape rate is thus computed as

$$\Gamma = \int_{\mathrm{TS}} J \cdot dS_{\perp}, \tag{2.13}$$

where the integral is over the transition surface, J is the probability flux normalized with respect to the partition function of the false vacuum (the "population" in the false vacuum), and $S_{\perp}$ a surface perpendicular to the transition surface. Computing the probability current, one sees that it splits into an equilibrium and nonequilibrium (σ) contributions as [42–46]

$$J = \sigma(u)\frac{e^{-S[\phi]}}{Z_{\mathrm{fv}}}, \tag{2.14}$$

where $\sigma(u)$ is a vector in phase space that parametrizes the deviation from equilibrium due to thermal fluctuations near the HM solution. This vector depends on $u = U(\phi - \phi_{\mathrm{top}}) + \bar{U}\pi$, where π is the momentum conjugate of ϕ, which describes linear fluctuations around the HM profile. Note that, as explained in Sec. II B 2, the suppression given by the Euclidean action $S[\phi]$ is equivalent to the standard $\beta E[\phi]$ Boltzmann suppression since we are working with a compact space of Hubble volume size over a Hubble time.

The integral in Eq. (2.13) can be rewritten as an integral of the current over the phase space restricted to the negative eigenmode subspace which parametrizes the transition surface. Thus, the flux over population method leads to a decay rate that factorizes into an equilibrium and a nonequilibrium contribution [42–46]. After performing a saddle-point approximation, the one-loop HM decay rate is given by

$$\Gamma = \frac{\kappa}{2\pi}\left|\frac{\det S''(\phi_{\mathrm{top}})}{\det S''(\phi_{\mathrm{fv}})}\right|^{-1/2} e^{-B} \quad \text{for } 2\pi T > \kappa. \tag{2.15}$$

In analogy to the quantum mechanical case [29], we assume that this large temperature behavior breaks down at $T = \kappa/(2\pi)$ which corresponds to the transition to the Coleman-de Lucia instanton. The factor of $\kappa/(2\pi)$ is the nonequilibrium contribution, commonly referred to as the dynamical factor, where κ is the growth rate of the unstable mode at the saddle point. It arises from the integration over the momenta conjugate to the negative mode in field space. To compute the dynamical prefactor, we look at the scalar field equation of motion which is given by Eq. (2.12). Expanding the scalar field ϕ in a series around ϕ_{top} and taking the ansatz $\phi - \phi_{\mathrm{top}} = Ce^{\kappa t}$, one finds that

$$\kappa = -\frac{3}{2}H\left(1 - \sqrt{1 + \frac{4|V''_{\mathrm{top}}|}{9H^2}}\right). \tag{2.16}$$

In obtaining the result above, we have assumed that the field gradients and the noise term are subdominant. We highlight that we can obtain an analytic solution for the prefactor in the Hawking-Moss case since the saddle point is given by a constant, but this not the case in more general situations. In several applications where dissipation can be neglected, the dynamical factor can be shown to be given by the negative eigenvalue. This can not be done in our case because the dissipation, given by the damping coefficient η, is proportional to the Hubble parameter which cannot be much smaller than $\sqrt{|V''_{\mathrm{top}}|}$, see Eq. (2.7). Taking the small dissipation limit is equivalent to taking $|V''_{\mathrm{top}}|/H^2 \gg 1$. In this limit, κ approaches the HM negative eigenvalue $\sqrt{|V''_{\mathrm{top}}|}$, but the Hawking-Moss instanton does not describe tunneling anymore. One can also note that the HM-CdL transition occurs as we approach the limit $\kappa = H$. In the large temperature (large friction) limit we have $\ddot{\phi} \ll 3H\dot{\phi}$ which leads to the simplified expression for the prefactor

$$\kappa^{\text{high T}} = \frac{|V''_{\mathrm{top}}|}{3H}. \tag{2.17}$$

4. Matching to stochastic formalism

Once we have a computation of the Hawking-Moss decay rate including the prefactor [Eq. (2.15)] we can compare our result to the stochastic formalism within the regime where the saddle-point approximation is valid. Before doing so, we highlight some similarities and fundamental differences between both approaches. While both approaches rely on the description given by a Langevin equation, the fundamental differences arise in the presence of the gradient term, the interpretation of the noise term, and the physics they capture. On the stochastic formalism case, there is no gradient term and the noise captures the physics of the short-wavelength modes of the scalar field. It further takes an overdamped approximation which leads to the Fokker-Planck equations with a Gaussian noise. Hence, it only capture classical physics. Meanwhile, in the thermal interpretation of the Hawking-Moss solution, the noise encodes the thermal modes. The thermal effective field theory captures quantum effects in a fixed de Sitter background. In Eq. (2.15) the one-loop effects are captured by the prefactor; this can be seen by restoring factors of $\hbar$ and moving the prefactor to the exponential. By doing so, it is clear that the prefactor corresponds to $\hbar$ corrections to the action.

By matching the decay rate computed in both approaches in the saddle-point approximation, we can understand how to capture quantum corrections in the stochastic formalism. To do so, we write the decay rate in Eq. (2.15) explicitly as

$$\Gamma = \frac{\kappa}{2\pi}\frac{\sqrt{V''_{\mathrm{fv}}}}{\sqrt{|V''_{\mathrm{top}}|}}\frac{\int \prod_{n\neq 0}\frac{\mathrm{d}c_n^{\mathrm{top}}}{\sqrt{2\pi}} e^{-S_{\mathrm{top}} - \frac{1}{2}\sum_{n\neq 0}(c_n^{\mathrm{top}})^2\lambda_n^{\mathrm{top}}}}{\int \prod_{n\neq 0}\frac{\mathrm{d}c_n^{\mathrm{fv}}}{\sqrt{2\pi}} e^{-S_{\mathrm{fv}} - \frac{1}{2}\sum_{n\neq 0}(c_n^{\mathrm{fv}})^2\lambda_n^{\mathrm{fv}}}}, \tag{2.18}$$

where we have expanded the field as $\phi = \phi_i + \sum_n c_n^i \psi_n$, with ψ_n the eigenfunctions of S'', $i = \{\text{top}, \text{fv}\}$, and rewritten the integration measure in terms of the coefficients c_n. Furthermore, we integrated over the homogeneous modes ψ_0. This is useful since it will allow us to rewrite expression in terms of an effective potential.

Note that when the volume of space is finite, such as in the Euclidean de Sitter case considered here, finite volume effects mean that different definitions of the effective potential are not equivalent contrary to the infinite volume case [47]. An intuitive definition that coincides with the usual derivation from 1PI diagrams in the infinite volume case is the constraint effective potential [47,48]. It introduces a δ function in the functional integral making the field ϕ have a constant expectation value and it is given by

$$e^{-\int \mathrm{d}^4 x U^{1\,\text{loop}}} = \int \mathrm{d}\phi e^{-S[\phi]} \delta\left(\frac{1}{\mathcal{V}}\int \phi \mathrm{d}^4 x - \phi_b\right) \overset{\text{one-loop}}{=} \int \prod_n \frac{\mathrm{d}c_n}{\sqrt{2\pi}} e^{-S - \frac{1}{2}\sum_n c_n^2 \lambda_n} \delta(c_0), \tag{2.19}$$

where the delta function in the second line tells us to integrate over the inhomogeneous modes only. We can now rewrite Eq. (2.18) using the constraint effective potential as

$$\Gamma = \frac{\kappa}{2\pi}\sqrt{\frac{V''_{\text{fv}}}{|V''_{\text{top}}|}} e^{-\frac{8\pi^2 \Delta U^{1\,\text{loop}}}{3H^4}}, \tag{2.20}$$

and in the high temperature limit ($|V''_{\text{top}}|/(4\pi^2) \ll T^2$), we find

$$\Gamma^{\text{high T}} = \frac{1}{2\pi}\frac{\sqrt{V''_{\text{fv}}|V''_{\text{top}}|}}{3H} e^{-\frac{8\pi^2 \Delta U^{1\,\text{loop}}}{3H^4}}. \tag{2.21}$$

The simplicity and validity of our analysis heavily relies on the fact that the Hawking-Moss solution is given by a constant saddle point, $\phi = \phi_{\text{top}}$. This allows for the simple interpretation of the escape rate as the tunneling rate, since both endpoints correspond to the top of the barrier. Similarly this avoids possible issues with double counting of modes when using the constraint effective potential since our saddle point is simply a constant [45,49].

We can now compare our result to the stochastic formalism one in the high temperature limit, which is equivalent to the small mass limit in which the stochastic formalism is valid. The difference with respect to the HM result arises from the fact that the HM result is a standard $4d$ field theoretical calculation while the stochastic formalism is a zero-dimensional field theory calculation. Thus, in the saddle-point approximation the stochastic formalism result does not include the ratio of functional determinants which are encoded in the constraint effective potential. Comparing Eq. (2.5) to Eq. (2.21) we see that the one-loop corrections can be encoded in the stochastic formalism by exchanging the potential V for the constraint one-loop effective potential $U^{1\,\text{loop}}$. Furthermore, we expect that the stochastic formalism, modified in this way to encode one-loop corrections, can now be applied beyond the saddle-point approximation.

In the following section, we will show with explicit examples that the HM calculation agrees with the stochastic approach in the region where both results are applicable. One should highlight again that the HM result is a saddle-point approximation. This approximation breaks down when perturbation theory ceases to be valid at either the top of the barrier or at the false vacuum. The latter corresponds to the region where $\Delta E < T$, that is, when the thermal fluctuations are large. In such region, we cannot have a metastable state localized in the false vacuum since the thermal fluctuations are large enough to destabilize it. Meanwhile the stochastic approach is not expected to be valid at large field masses due to the overdamped assumption. Outside of these regimes, both calculations of the decay rate agree, by construction, as long as we use the constraint effective potential in the stochastic approach.

III. COMPARISON BETWEEN STOCHASTIC AND THERMAL APPROACHES

In this section we will compare the results from the thermal HM decay rate calculation and the stochastic formalism one. For simplicity, we will consider that the one-loop constraint effective potential is given by

$$U(\phi) = 3H^2 M_{\text{Pl}}^2 + \mu^3\phi - \frac{1}{2}m^2\phi^2 - \frac{M}{3!}\phi^3 + \frac{\lambda}{4!}\phi^4 - \frac{\lambda_5}{5!H}\phi^5 + \frac{\lambda_6}{6!H^2}\phi^6. \tag{3.1}$$

In general, the shape of this potential will be given by a more complicated dependence on ϕ and should include a renormalization scale μ that arises after renormalizing the one-loop divergences. Nevertheless, this simple example is enough for our purposes of comparing the different calculations of the decay rate. We proceed to write the potential in terms of dimensionless variables. Defining

$$\alpha = \frac{m^2}{H^2\lambda^{1/2}}, \quad \beta = \frac{\mu^3}{H^3\lambda^{1/4}}, \quad \gamma = \frac{M}{H\lambda^{3/4}}, \quad \Lambda_5 = \frac{\lambda_5}{\lambda^{5/4}}, \quad \Lambda_6 = \frac{\lambda_6}{\lambda^{6/4}}, \quad x = \Omega\lambda^{1/4}\frac{\phi}{H}, \quad \Omega = 1 + \sqrt{\alpha} + \beta + \gamma^{1/3}, \tag{3.2}$$

the rescaled potential reads

$$\frac{v(z)}{\pi^2} = \frac{4M_{\rm Pl}^2}{H^2} + \frac{4\beta z}{3\Omega} - \frac{2\alpha z^2}{3\Omega^2} - \frac{2\gamma z^3}{9\Omega^3} + \frac{z^4}{18\Omega^4} - \frac{\Lambda_5 z^5}{90\Omega^5} - \frac{\Lambda_6 z^6}{540\Omega^6}. \tag{3.3}$$

We now analyze the decay rate for three different cases. The first one corresponds to a potential unbounded from below on one side, with a metastable vacuum where $\mu = \lambda = \lambda_6 = 0$. The dimensionless variables α, γ, and x are now defined as in Eq. (3.2) with $\lambda = 1$. The decay rate for this potential computed both from the thermal HM and stochastic approaches is shown in Fig. 1(a). We can see that the results agree for large masses which is the region where the thermal fluctuations are small and do not destabilize the unstable vacuum. In this region, the numerical calculation of the eigenvalues becomes difficult and analytic expression such as Eq. (2.20) becomes useful. At small masses, when the potential barrier becomes increasingly small, we can no longer trust the thermal HM calculation. Meanwhile, the stochastic result still describes the decay rate as long as an unstable vacuum exists. One should note that at very large masses (large α), the stochastic approach result becomes less precise, see Fig. 1(b). The massless limit assumed in the stochastic approach is equivalent to the high temperature limit result in Eq. (2.21), but the precise value of the decay rate receives corrections that grow with the curvature of the potential at the top of the barrier, as seen in Eq. (2.16).

Since solving the FP equation is equivalent to solving the Schrödinger equation for a supersymmetric Hamiltonian [50], we can use well-known results from zero-dimensional supersymmetry to understand the relation between the stochastic and the HM computations. In the stochastic approach, the decay rate is given by the lowest eigenvalue of the FP equation. Thus, given a potential v, the equation with the flipped potential, $-v$, will have the same lowest eigenvalue. This tells us that we can think of the decay rate as being computed for the flipped potential and that the decay rate should be symmetric under the exchange false vacuum $\leftrightarrow$ top of the barrier, which we see that is indeed the case at large temperatures [Eq. (2.21)].

The second case is a potential with a true and a false vacuum where $\gamma = \lambda_5 = \lambda_6 = 0$. We analyze this potential for different values of α and β and show our results in Fig. 2. As in the previous case, the thermal HM calculation breaks down at small α. Meanwhile, for large enough α and β where there is a clear distinction between the false and true vacuum, we see perfect agreement between the HM and stochastic approach. When we decrease β, the vacua are nearly degenerate. The HM result still describes the tunneling from the false vacuum to the true vacuum, given the boundary conditions chosen to solve the FP equation when computing the escape rate. On the other hand, the stochastic approach includes the fluctuation bouncing back from the true vacuum to the false vacuum. We can see this by looking again at the flipped potential $-v$. In that case there is a false vacuum (previously the top of the wall) with one wall on each side. Due to supersymmetry, the stochastic formalism will simply give the same result, while for the HM computation we have to account for the probability to transition to either side, or in other words double the decay rate. This is confirmed in the results from Fig. 2 where we compare twice the value of the HM decay rate from Eq. (2.20), with the numerical computation for the lowest eigenvalue of the FP equation.

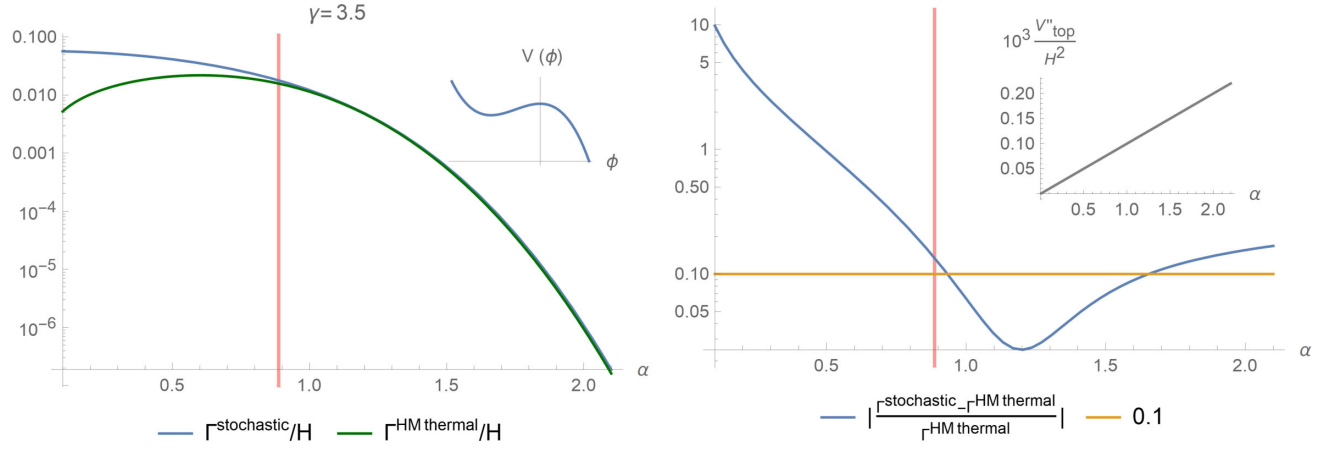

FIG. 1. Comparison of the decay rate for an unbounded potential with a metastable vacuum. We have taken the potential in Eq. (3.1) with $\beta = \lambda = \Lambda_6 = 0$, $H = 10^{-2}M_{\rm Pl}$, and $\lambda_5 = 10^{-4}$. For plot (a), the green line corresponds to Eq. (2.20) and the blue line is computed from the lowest eigenvalue of the Fokker-Planck equation in the stochastic approach. To the left of the vertical red line the saddle-point approximation breaks. In plot (b), we can observe that as α increases the discrepancy between the decay rates increases too. This is explained due to the increase in $V''_{\rm top}$.

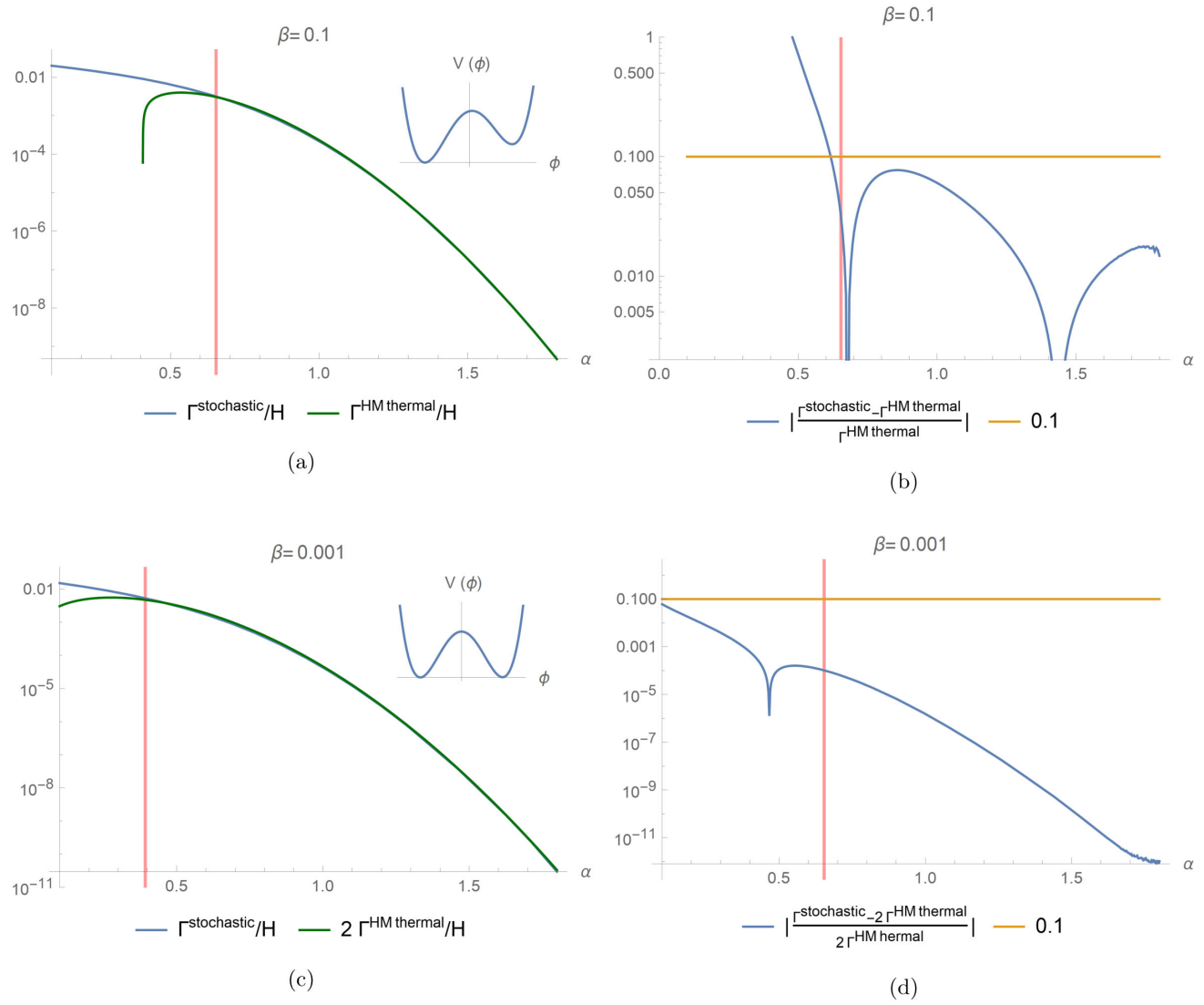

FIG. 2. Comparison of the decay rate of the false vacuum. We have taken the potential in Eq. (3.1) with $\gamma = \Lambda_5 = \Lambda_6 = 0$, $H = 10^{-3} M_{\rm Pl}$, and $\lambda = 0.05$. For plots (a) and (c), the green line is computed using Eq. (2.20) and the blue line is computed in the stochastic approach. Note that the sudden drop in the HM decay rate corresponds to the value of α where the potential ceases to have two vacua. To the left of the vertical red line (value at which $\Delta E = T$) the saddle-point approximation breaks. For plots (b) and (d), the blue line shows the discrepancy between the stochastic and instanton approach, we can see that for the present cases it is always small to the right of the red vertical line.

We consider a third case which will demonstrate the breaking of the HM result due to the non-Gaussianity of the path integral at the top of the barrier. In this case, we take a potential with $\alpha = \gamma = \lambda_5 = 0$. The parameter β measures the curvature at the top of the barrier, as we take $\beta \to 0$, $V''_{\rm top}$ vanishes. Since we have $V''_{\rm top} \ll V^{(4)}_{\rm top}$, perturbation theory, and hence the saddle-point approximation break. This is observed in Fig. 3 where the HM result largely deviates from the stochastic one as we decrease the coefficient of the linear term.

Last, we analyze in detail the regions where the validity of the saddle-point approximation breaks. As a first step, we should find the region where $\Delta E/T < 1$. In principle, this requires knowledge of the tree-level potential, which we do not have for the present examples. Nevertheless, if we assume perturbation theory is valid then $\Delta E/T \sim \Delta E^{1\,\rm loop}/T$, where the one-loop difference in energies is given by the difference between the constraint effective potential evaluated at the top of the barrier and at the false vacuum. Thus, the region where perturbation theory is valid and the saddle-point approximation holds corresponds to $\Delta E^{1\,\rm loop}/T > 1$. Another possibility for the failure of the saddle-point approximation is the breaking of perturbation theory. For the first two examples analyzed here, we can see that the breaking of perturbation theory at the false vacuum happens when $T < E^{1\,\rm loop} \sim m^4/(\lambda H^3)$,

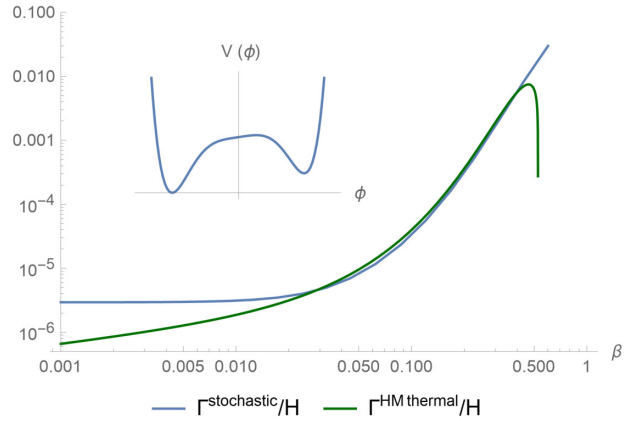

FIG. 3. Breakdown of the thermal HM result. We have taken $H = 10^{-3}M_{\text{Pl}}$, $\lambda = -0.3$, and $\lambda_6 = 60$. For small values of β, the path integral at the top of the barrier is non-Gaussian due to the curvature becoming extremely small. At large β the potential seizes to have two vacua; this happens when the HM result suddenly drops.

that is at small α. In fact, the lack of exponential suppression for the decay rate, which can be understood as thermal fluctuations becoming large and destabilizing the false vacuum, is equivalent to the non-Gaussianity of the path integral at the false vacuum. In this regime, the decay rate computed from the HM bounce is not valid; this can be observed in Figs. 1(a) and 2. The second region where the saddle-point approximation breaks corresponds to the breaking of perturbation theory near the top of the barrier. In the third case analyzed above, this happens when the curvature at the top of the potential approaches zero (see Fig. 3). On the other hand, the stochastic approach assumptions break down at higher masses, i.e. higher α, since the over-damped approximation is used when solving the Langevin equation. In this regime, the prefactor receives corrections that grow with the curvature at the top of the barrier as seen in Fig. 1(b).

IV. DISCUSSION

In this article, we computed an explicit analytic formula for the decay rate in a de Sitter space at high Hubble rates using the Hawking-Moss instanton approximation including one-loop quantum corrections. We then showed that the stochastic Starobinsky-Yokoyama approach reproduces the Hawking-Moss result when the one-loop constraint effective potential is used instead of the classical potential, in the regime where both calculations are valid, that is, when the saddle-point approximation holds at both the false vacuum and the top of the barrier, and the curvature of the potential is smaller than the Hubble rate. It is important to note that because of the finite volume of the de Sitter space, different definitions of effective potential are not equivalent. For example, the more commonly used perturbative effective potential is not equal to the constraint effective potential.

Our results suggest that the stochastic approach with the constraint effective potential can give a non-perturbative way of computing vacuum decay rates when the saddle-point approximation, which the Hawking-Moss calculation relies on, is not valid. Correspondingly, we show that the stochastic method, which relies on the overdamped assumption, fails when the curvature of the potential becomes comparable to the Hubble rate. Meanwhile, the Hawking-Moss calculation is valid in this regime. Therefore, both methods are needed for a complete description of vacuum decay in de Sitter spacetimes at high Hubble rates.

ACKNOWLEDGMENTS

We would like to thank Oliver Gould and Stephen Stopyra for useful discussions. All authors were supported by STFC Grant No. ST/P000762/1, and M. C. G. and A. R. also by the STFC Grant No. ST/T000791/1. M. C. G. was supported by the European Union's Horizon 2020 Research Council Grant No. 724659 MassiveCosmo ERC–2016–COG. J. E. C. was supported by the Carl Trygger Foundation through Grant No. CTS 17:139.

[1] S. Chatrchyan *et al.* (CMS Collaboration), Phys. Lett. B **716**, 30 (2012).
[2] G. Aad *et al.* (ATLAS Collaboration), Phys. Lett. B **716**, 1 (2012).
[3] S. Chigusa, T. Moroi, and Y. Shoji, Phys. Rev. Lett. **119**, 211801 (2017).
[4] S. Chigusa, T. Moroi, and Y. Shoji, Phys. Rev. D **97**, 116012 (2018).
[5] A. Rajantie and S. Stopyra, Phys. Rev. D **95**, 025008 (2017).
[6] J. R. Espinosa, J. Cosmol. Astropart. Phys. 06 (2020) 052.
[7] V. Branchina and E. Messina, Phys. Rev. Lett. **111**, 241801 (2013).
[8] T. Markkanen, A. Rajantie, and S. Stopyra, Front. Astron. Space Sci. **5**, 40 (2018).
[9] S. Coleman, Phys. Rev. D **15**, 2929 (1977).
[10] C. G. Callan, Jr. and S. R. Coleman, Phys. Rev. D **16**, 1762 (1977).
[11] E. J. Weinberg, Phys. Rev. Lett. **98**, 251303 (2007)..
[12] E. J. Weinberg, *Classical Solutions in Quantum Field Theory: Solitons and Instantons in High Energy Physics*,

Cambridge Monographs on Mathematical Physics (Cambridge University Press, Cambridge, England, 2012).
[13] A. R. Brown and E. J. Weinberg, Phys. Rev. D **76**, 064003 (2007).
[14] S. R. Coleman and F. De Luccia, Phys. Rev. D **21**, 3305 (1980).
[15] L. G. Jensen and P. J. Steinhardt, Nucl. Phys. **B237**, 176 (1984).
[16] S. W. Hawking and I. G. Moss, Phys. Lett. **110B**, 35 (1982).
[17] A. A. Starobinsky, Lect. Notes Phys. **246**, 107 (1986).
[18] A. A. Starobinsky and J. Yokoyama, Phys. Rev. D **50**, 6357 (1994).
[19] J. E. Camargo-Molina and A. Rajantie, arXiv:2204.02875.
[20] J. Fumagalli, S. Renaux-Petel, and J. W. Ronayne, J. High Energy Phys. 02 (2020) 142.
[21] I. Moss and G. Rigopoulos, J. Cosmol. Astropart. Phys. 05 (2017) 009.
[22] V. Vennin and A. A. Starobinsky, Eur. Phys. J. C **75**, 413 (2015).
[23] R. J. Hardwick, V. Vennin, C. T. Byrnes, J. Torrado, and D. Wands, J. Cosmol. Astropart. Phys. 10 (2017) 018.
[24] H. Risken and H. Haken, *The Fokker-Planck Equation: Methods of Solution and Applications Second Edition* (Springer, New York, 1989).
[25] P. Hänggi, P. Talkner, and M. Borkovec, Rev. Mod. Phys. **62**, 251 (1990).
[26] P. Reimann, G. J. Schmid, and P. Hänggi, Phys. Rev. E **60**, R1 (1999).
[27] T. Tanaka and M. Sasaki, Prog. Theor. Phys. **88**, 503 (1992).
[28] G. W. Gibbons and S. W. Hawking, Phys. Rev. D **15**, 2738 (1977).
[29] I. Affleck, Phys. Rev. Lett. **46**, 388 (1981).
[30] A. D. Linde, Nucl. Phys. **B216**, 421 (1983); **B223**, 544(E) (1983).
[31] A. Linde, Phys. Lett. **100B**, 37 (1981).
[32] V. Gorbenko and L. Senatore, arXiv:1911.00022.
[33] M. Spradlin, A. Strominger, and A. Volovich, in *Les Houches Summer School: Session 76: Euro Summer School on Unity of Fundamental Physics: Gravity, Gauge Theory and Strings* (2001), pp. 423–453.
[34] D. Anninos, Int. J. Mod. Phys. A **27**, 1230013 (2012).
[35] A. H. Mueller and D. T. Son, Phys. Lett. B **582**, 279 (2004).
[36] C. Greiner and B. Muller, Phys. Rev. D **55**, 1026 (1997).
[37] G. Aarts and J. Smit, Nucl. Phys. **B511**, 451 (1998).
[38] D. Bodeker, Nucl. Phys. **B486**, 500 (1997).
[39] A. H. Guth and S.-Y. Pi, Phys. Rev. D **32**, 1899 (1985).
[40] C. P. Burgess, R. Holman, G. Tasinato, and M. Williams, J. High Energy Phys. 03 (2015) 090.
[41] C. P. Burgess, R. Holman, and G. Tasinato, J. High Energy Phys. 01 (2016) 153.
[42] H. A. Kramers, Physica (Utrecht) **7**, 284 (1940).
[43] J. Langer, Ann. Phys. (N.Y.) **54**, 258 (1969).
[44] A. Berera, J. Mabillard, B. W. Mintz, and R. O. Ramos, Phys. Rev. D **100**, 076005 (2019).
[45] O. Gould and J. Hirvonen, Phys. Rev. D **104**, 096015 (2021).
[46] A. Ekstedt, J. High Energy Phys. 08 (2022) 115.
[47] L. O'Raifeartaigh, A. Wipf, and H. Yoneyama, Nucl. Phys. **B271**, 653 (1986).
[48] R. Fukuda and E. Kyriakopoulos, Nucl. Phys. **B85**, 354 (1975).
[49] D. Croon, O. Gould, P. Schicho, T. V. I. Tenkanen, and G. White, J. High Energy Phys. 04 (2021) 055.
[50] F. Cooper, A. Khare, and U. Sukhatme, Phys. Rep. **251**, 267 (1995).